AIAA 81-0046R

Solutions of the Compressible Navier-Stokes Equations Using the Integral Method

M. M. ElRefaee,* J. C. Wu,† and S. G. Lekoudis‡
Georgia Institute of Technology, Atlanta, Ga.

The integral representation method was used to obtain numerical solutions of the compressible, unsteady, two-dimensional Navier-Stokes equations for subsonic flows. The equations were written with the vorticity, the dilatation, the density, and the enthalpy as the dependent variables. The method was tested by solving the following problems: the flow over a flat plate, around a circular cylinder, and around a Joukowski airfoil. The last two problems involved massive flow separation. The approach offers the capability of confining the domain of computations to the region where two quantities, the vorticity and the difference in dilatation between the real flow and the potential flow around the body, are non-negligible.

I. Introduction

THE equations that govern most of the flows of interest in aerodynamic applications are the Navier-Stokes equations. Because of their complexity, analytical solutions are available only for an extremely small number of problems. Hence, numerical solutions are being sought. For flowfields with certain characteristics, simplifications of the Navier-Stokes equations, compatible with the characteristics, have been used to predict these flowfields. However, there are cases of importance in applications where simplifications of the equations are not allowed because of the nature of the flowfield. Examples of such cases are the static and dynamic stalls of airfoils and the complicated flows inside turbomachinery devices.

The computation of the flowfield around airfoils undergoing static or dynamic stall has already been performed by several investigators. References 1-6 describe different methods for solving the problem in incompressible flow. The compressible flow problem has been examined in Refs. 7 and 8. These calculations require considerable resources, especially for the case of high Reynolds number flows. Some of the reasons for the requirements will be explained subsequently.

Most of the methods used to obtain numerical solutions to the Navier-Stokes equations have common characteristics. They use finite-difference techniques and they apply the infinity boundary conditions at some finite distance from the body. They compute the surface vorticity, a quantity of importance in the accuracy of the calculations, using essentially interpolation procedures. One reason that it is costly to obtain these solutions is that a large number of grid points must be used. That is so because the grid must capture the details of the flow where the gradients are large and also extend far enough so that the infinity boundary conditions can be used with some confidence.

A different approach for computing unsteady viscous flowfields was presented in Refs. 9 and 10. The main advantages of this approach, called the integral representation method, are the following. First, the computations are confined to regions of non-negligible vorticity, which are quite small for high Reynolds number flows. Hence, the number of points in the computational grid is smaller than the number required by more conventional approaches for comparable accuracy. Second, the surface vorticity is computed directly and not through interpolation. Moreover, the infinity boundary conditions are satisfied exactly. For the case of incompressible flows, the flowfield around airfoils with massive separation was computed using this approach in Refs. 2-6.

In the present study, the integral approach is extended to compressible flows. This has been achieved by using the dilatation as a dependent variable. The resulting system of equations needs to be solved only where the vorticity and the dilatation are non-negligible. Because the dilatation is significant at distances from the body where the vorticity is already negligible at high Reynolds numbers, the approach initially does not seem as advantageous as in the incompressible case. However, the problem has been reformulated so that solutions are needed only in regions where the vorticity is non-negligible and the dilatation difference between the viscous flow and the potential flow around the same configuration is also non-negligible.

The developed formulation has been applied to the following problems. The problem of the flow over a flat plate, around a circular cylinder, and around an airfoil. The last two problems involve massive flow separation. The formulation is described in Sec. II of this paper. The numerical procedure used is described in Sec. III, the results and discussion are in Sec. IV, and the conclusions are in Sec. V.

II. Analytical Formulation

A. Governing Equations

In an unbounded two-dimensional region R, the conservation of mass for compressible flow can be expressed as[13]

$$V(r,t) = \frac{1}{2\pi}\int_R \frac{\omega(r_0,t)\times(r-r_0)+\beta(r_0,t)\,(r-r_0)}{|\,r-r_0\,|^2}\,dR + V_\infty \tag{1}$$

where

$$\omega(r,t) = \nabla \times V(r,t) \tag{2a}$$

$$\beta(r,t) = \nabla \cdot V(r,t) \tag{2b}$$

are the definitions of vorticity ω and dilatation β, and V_∞ is the assumed uniform velocity at infinity. Equations (1) and (2) describe the kinematics of the flow because, once ω and β are known, the instantaneous velocity field is known everywhere through the integral Eq. (1). In the incompressible

Presented as Paper 81-0046 at the AIAA 19th Aerospace Sciences Meeting, St. Louis, Mo., Jan. 12-15, 1981; submitted Feb. 19, 1981; revision received July 17, 1981.

*Post-Doctoral Fellow, School of Aerospace Engineering. Student Member AIAA.

†Professor, School of Aerospace Engineering. Associate Fellow AIAA.

‡Assistant Professor, School of Aerospace Engineering. Member AIAA.

flow case, the vorticity ω is governed by the vorticity transport equation, obtained by applying the curl operator on the momentum equation (Navier-Stokes equation) and using Eq. (2a). In the compressible case, $\beta \neq 0$, an equation governing the transport of the dilatation β is needed. Using the definitions Eqs. (2) and applying the curl and the divergence operators on the compressible momentum equation for two-dimensional flow, obtain

$$\frac{\partial \omega}{\partial t} = -V\cdot\nabla\omega + \left(\frac{\mu}{\rho R_e}\right)\nabla^2\omega + \phi(\rho,\beta,\omega,h) \tag{3}$$

$$\frac{\partial \beta}{\partial t} = -V\cdot\nabla\beta + \left(\frac{4/3\mu}{\rho R_e}\right)\nabla^2\beta + \psi(\rho,\beta,\omega,h) \tag{4}$$

where ω denotes the magnitude of vorticity vector. The terms ϕ and ψ are given in the Appendix, look like "source" terms, and are identically zero in the incompressible case. In Eqs. (3) and (4) R_e is the Reynolds number, ρ the density, μ the (variable) viscosity, and h the enthalpy. Hence, it seems necessary, in order to solve the system Eqs. (1-4) and obtain answers to the problem of compressible flow, to have ρ and h available. They can be obtained by solving the following equations for ρ and h:

$$\frac{\partial \ell n\rho}{\partial t} = -V\cdot\nabla\ell n\rho - \beta \tag{5}$$

$$\frac{\partial h}{\partial t} = -V\cdot\nabla h + \left(\frac{\gamma k}{\rho R_e Pr}\right)\nabla^2 h + \theta(\rho,\beta,h,\omega) \tag{6}$$

The governing Eqs. (3-6) have been nondimensionalized by normalizing the variable with respect to the following reference quantities: distance L, velocity V_∞, density ρ_∞, enthalpy V_∞^2, and time L/V_∞ where L is the characteristic length of the body. The expression Eq. (5) is the conservation of mass and Eq. (6) is the energy equation. θ, ϕ, and ψ are source terms and are given in the Appendix. In Eq. (6), the perfect gas equation of state is used, Pr is the Prandtl number, k the thermal conductivity, and γ the ratio of specific heats. The system of Eqs. (1-6) is closed and completely equivalent to the familiar Navier-Stokes equations written in primitive variables, provided that the dependence of Pr, μ, k, and γ on the state properties ρ and h is known. The following observation can be made about this system.

Because Eqs. (1) and (2) completely define the flowfield (the instantaneous pressure can be obtained easily through a numerical integration of the momentum equation once the velocities are known) we need only to solve for the part of the flowfield where ω and β are non-negligible. For high Reynolds number flows, ω is substantial only in a region close to the body and in the wake. Hence this approach offers a reduction of the computational region, compared with more conventional formulations. This has already been demonstrated in calculations of problems involving incompressible flows.[2-6] In the compressible flow problem examined here, the computational domain must extend far enough from the body to include the region where β is substantial, at least in the computational sense. For the case of the subsonic flow around an airfoil, potential flow theory indicates that this region has a length scale comparable with the airfoil chord. Hence, it seems that the developed formulation does not offer any substantial advantage over the more conventional approaches. However, by using potential flow solutions around the body, it will be shown in Sec. B that the domain of computations can be further reduced.

B. Use of Potential Flow Solution

Equation (1) can be written in the following form:

$$V(r,t) = \frac{1}{2\pi}\int_{R_1}\frac{\omega(r_0,t)\times(r-r_0)+\beta(r_0,t)\,(r-r_0)}{|r-r_0|^2}\,dR + \frac{1}{2\pi}\int_{R_2}\frac{\beta(r_0,t)\,(r-r_0)}{|r-r_0|^2}\,dR + V_\infty \tag{7}$$

where R_1 is the region of the flow where vorticity is non-negligible and R_2 is the rest of the domain, extending to infinity for exterior flow problems. This expression can be written for potential flows around the same body

$$V_p(r,t) = \frac{1}{2\pi}\int_{R_1}\frac{\beta_p(r_0,t)\,(r-r_0)}{|r-r_0|^2}\,dR + \frac{1}{2\pi}\int_{R_2}\frac{\beta_p(r_0,t)\,(r-r_0)}{|r-r_0|^2}\,dR + \frac{1}{2\pi}\int_S\frac{\gamma_p\times(r-r_0)}{|r-r_0|^2}\,dS + V_\infty \tag{8}$$

where the subscript p indicates potential flow and γ_p is the vortex sheet strength on the surface S of the body, due to the potential flow. Then, if R_1 extends far enough from the body, the combination of Eqs. (7) and (8) gives

$$V(r,t) = \frac{1}{2\pi}\int_{R_1}\frac{\omega\times(r-r_0)+(\beta-\beta_p)\,(r-r_0)}{|r-r_0|^2}\,dR - \frac{1}{2\pi}\int_S\frac{\gamma_p\times(r-r_0)}{|r-r_0|^2}\,dS + V_p \tag{9}$$

The relation Eq. (9) implies the following. First $\beta-\beta_p$ in R_2 is small enough so that its effect on the velocity in R_1 is negligible. Second, one needs to solve only in R_1, which is a smaller region than the region where β is significant. Thus, the approach does offer a reduction of the computational domain, compared with conventional approaches.

A study has been conducted to determine the contribution of the dilatation difference, $\beta-\beta_p$, in region R_2 to the velocities in region R_1 (vortical region). The difference in dilatation between the viscous flow and the potential flow around a circular cylinder is simulated by a difference in dilatation between two potential flows, one around a circle and the other around an ellipse. The ellipse acted as a fictitious body surrounding the vortical region. A series solution in Mach number ($M<1$) was then used to get the value $\beta_{\text{circle}}-\beta_{\text{ellipse}}$ from the known incompressible solutions around the circle and the ellipse. The contribution of $\beta_{\text{circle}}-\beta_{\text{ellipse}}$ in region R_2 to the velocities R_1 was calculated by using the integral relation.[11] The results obtained indicated that if the region R_1 extends far enough, the contribution of $\beta_{\text{circle}}-\beta_{\text{ellipse}}$ in R_2 to the velocities in R_1 becomes negligible. Detailed discussion is given in Ref. 11. For example if R_1 extends 5 radii away from the circle, the contribution of the value $\beta_{\text{circle}}-\beta_{\text{ellipse}}$ in R_2 to the velocities in R_1 becomes less than 1% of the freestream velocity.

C. Surface Vorticity

Imposing the no-slip condition on the body surface overspecifies the boundary condition for the vorticity transport equation. This statement has already been discussed in detail in other publications dealing with the integral representation approach, and a detailed description can be found in Ref. 10. It can be shown[10] that a unique determination of the surface vorticity can be made by applying the no-slip condition on the integral expression for the kinematics of the problem. For the case of the compressible flow problem

examined here, the application of the no-slip condition on Eq. (9) gives

$$\int_S \frac{(\gamma-\gamma_p)\times(r_s-r_0)}{|r_s-r_0|^2}\,dS+\int_{R_1}\frac{(\beta-\beta_p)(r_s-r_0)}{|r_s-r_0|^2}\,dR + \int_{R_1-S}\frac{\omega\times(r_s-r_0)\,dR}{|r_s-r_0|^2}=0 \tag{10}$$

where the subscript S denotes the solid boundary and γ is the unknown surface vorticity, to be obtained by solving the integral Eq. (10) for γ.

Equation (10) is a vector equation. An efficient method to solve Eq. (10) for γ has been developed and applied to the incompressible flow case. To describe the method briefly, the dot product of Eq. (10) with the vector t, tangential to the body surface, is taken and the principle of conservation of total vorticity is used to transfer γ outside the first integral. The area integrals involving ω are evaluated using Fourier series expansion because the flow is periodic in θ, in a polar coordinate system (r,θ). This applies both to the cylinder and to airfoil problems because the computational domain for the airfoil is the outside of the cylinder to which the airfoil is transformed. The same technique has been used in the present study with the extra complication of evaluating the area integrals involving the dilatation using Fourier series. Details can be found in Ref. 11.

III. Numerical Procedures

Because the computation of the flow around the airfoil is the most complicated of the problems that have been attacked using the formulation described in Sec. II, the subsequent discussion will be confined to this case.

The region around the Joukowski airfoil was transformed onto the region outside a circular cylinder through a conformal transformation.[11] Hence, for both the cylinder and the airfoil problems, the computational domain was the same. In this domain a polar coordinate system (r,θ) was used. For the case of the airfoil, the governing equations are the same as in the case of the circular cylinder, the only difference being the appearance of the scale factor of the transformation. This procedure, used several times before in the solution of incompressible flow problems, can be found in Refs. 4, 5, and 11.

For reasons of computational efficiency, the integral representation for the kinematics was used only in a part of the computational domain. This part included the outer boundary, the first eight grid lines around the airfoil, and a region between the airfoil and the downstream boundary. This region was bounded by two grid lines in the radial direction and included the trailing edge of the airfoil. In the rest of the computational domain, a Poisson equation for the velocity in the θ direction was solved. Then, the definition of the dilatation β was used to obtain the velocity in the r direction.

The transport equations for ω, β, ρ, and h, Eqs. (3), (4), (5), and (6), respectively, have the same form. Hence, the numerical scheme used to solve them is kept identical. The equations were solved in the computational domain using a polar grid with equal spacing in θ, and increasing spacing in the radial direction according to

$$r_j = C+\exp[z_0+(j-1)\Delta z] \tag{11}$$

with the cylinder radius having a length of unity and j increasing away from the cylinder. An implicit finite-difference scheme was used for the solution of the transport equations. The time derivative was approximated using first-order backward differencing and the diffusion and source terms were approximated using second-order central differencing at the solution time level. The convection terms were approximated, in their conservation form, by second order[14] upwind differencing. The finite-difference equations were linearized by delaying the velocities at the convection terms by one time step, and by delaying some quantities in the source terms. The resulting algebraic equations were solved using a successive "point under-relaxation" scheme. The relaxation sweeps were alternating in the θ direction because that was found to accelerate convergence. The solid body was set into motion impulsively. At this impulsive start, the flow was prescribed by the potential flow solution. The sequence of the calculations was as follows.

1) With all the dependent variables known at the previous time level, the vorticity transport equation is solved to obtain the values of the interior vorticity.

2) New values of the boundary vorticity are obtained using the integral representation, as described in Sec. II.C. The steps 1 and 2 are repeated until a prescribed convergence criterion is satisfied.

3) The rest of the transport equations are solved to determine the values of ρ, β, and h at the new time level.

4) Using the new ω and β, the velocities are computed in the θ direction. As mentioned before, the integral relationship is used for the first eight grid lines next to the body, at the outer boundary, and at a region that includes the trailing edge of the airfoil and is bounded by two grid lines in the radial direction. In the rest of the domain, a Poisson equation is solved for the velocity in the θ direction using finite differences. Then the velocities in the r direction are obtained using the definition of the dilatation. The time is advanced and the procedure is repeated from step 1.

The zero derivative of h and ρ normal to the wall was used as the boundary condition (adiabatic wall). The value of β at the wall was obtained using three-point extrapolation at each iteration of the transport equation for β. The potential flow values used for all the field variables were used as upstream boundary conditions at the outer boundary. Zero second derivatives for h, ρ, and β, and zero vorticity were used as downstream boundary conditions at the outer boundary. The wake never approached the outer boundary during the calculations. The convergence criteria used in solving the vorticity transport equation were based on the maximum variation of the surface vortex strength between two consecutive iterations. At early time levels this tolerance was specified to be 0.002 and subsequently is reduced to 0.0005 at later time levels.

IV. Results and Discussion

The formulation presented in Sec. II of this paper was tested by solving for the flow over a flat plate, around a circular cylinder, and around a 9%-thick symmetric Joukowski airfoil. A description of the results follows.

The flow over a flat plate was solved for the following conditions: freestream Mach number 0.5, Prandtl number 1,

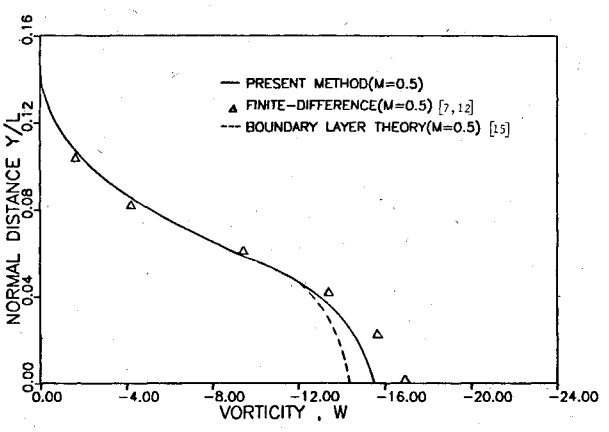

Fig. 1 Surface vorticity at midplate.

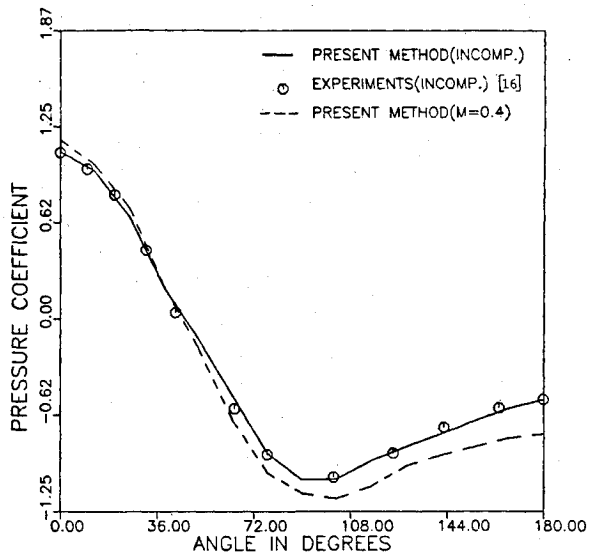

Fig. 2 Pressure distribution comparison (compressibility effect) on circular cylinder.

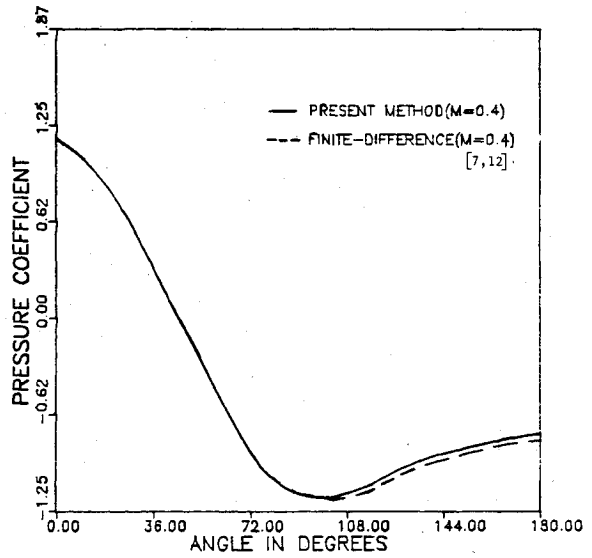

Fig. 3 Pressure distribution on circular cylinder (comparison between the present method and the pure finite-difference method).

Table 1 Comparison between finite-difference method and present method

Quantity	Finite-differences [12]	Present method
Angle of separation, deg	127.5	126.3
Length of standing vortex over cylinder diameter	2.54	2.92
Drag coefficient due to pressure	1.32	1.23
Drag coefficient due to shear	0.561	0.520

Reynolds number based on plate length 1000. A relatively coarse grid with uniform $\Delta x = 0.1L$, $\Delta y = 0.04L$ was used. The grid extended $0.5L$ ahead of the leading edge of the plate, $1.5L$ behind the trailing edge of the plate, and $0.8L$ above the plate. Figure 1 shows the vorticity at the middle of the plate obtained using the present formulation, a purely finite-difference technique, and a boundary-layer theory.[11,12,15] The differences are due partly to the different grids and partly to

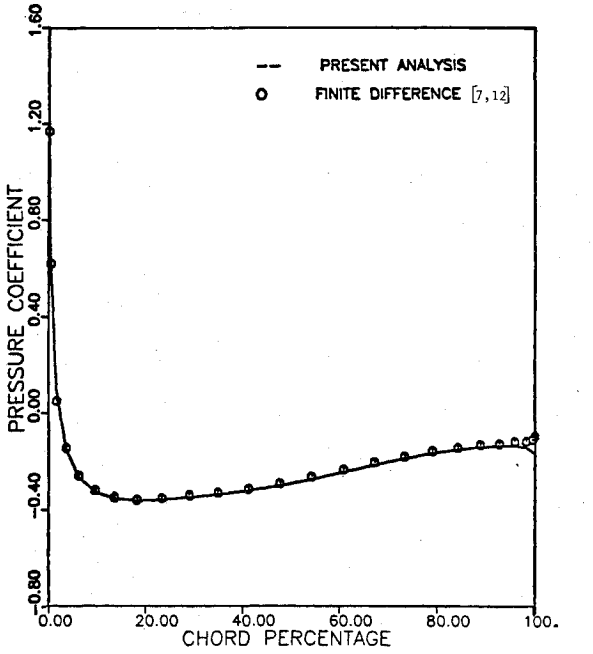

Fig. 4 Surface pressure distribution on a 9% Joukowski airfoil at zero angle of attack.

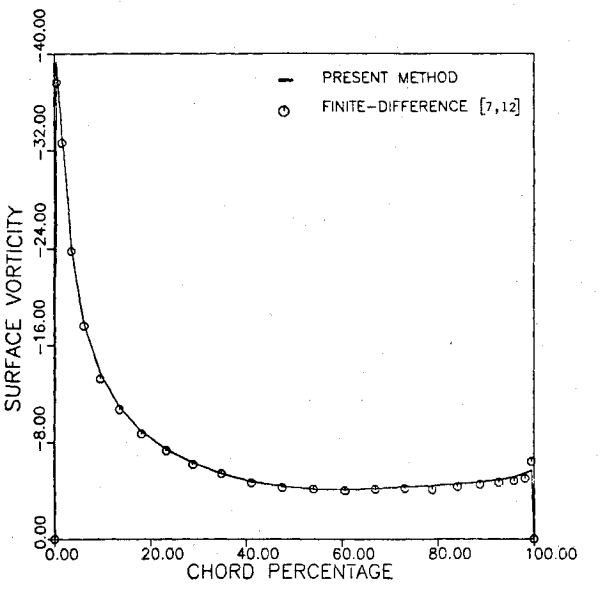

Fig. 5 Surface vorticity distribution on a 9% Joukowski airfoil at zero angle of attack.

the different numerical schemes used. The overshoot of the present result over the boundary-layer data near the surface is expected and is due to the favorable pressure gradient along the surface caused by the displacement effect.

The second test problem solved was the flow over a circular cylinder. The conditions used were the following: freestream Mach number 0.4, Prandtl number 1, Reynolds number based on the cylinder diameter 40. The grid consists of lines of constant radii and lines of constant angle θ. The lines of constant θ are equally spaced with $\pi/20$ intervals. In the radial direction, an exponential stretching relation is assumed $r = \exp[0.06(j-1)]$. The total number of grid points used is 2000. At the earlier time levels, the computational region contained about 40% of the total number of points. As the solution progressed in time, the number of points in the computational domain gradually increase. The computations were started by using the potential flow solution at the

beginning and stopped at a time level of 7.5, based on the freestream velocity and the cylinder diameter, when numerically steady state was achieved. The CPU time used to reach steady state is 8 min on a CDC 6600 computer. To test the program, the vorticity transport equation was solved alone by "switching off" the source terms. Thus, incompressible flow results were obtained. Figure 2 shows a comparison of the pressure coefficient obtained using the developed formulation, obtained for the incompressible flow case, and for experiments in incompressible flows.[16] The compressibility effect is present. Although the freestream Mach number is 0.4, the local Mach number reaches almost unity near the shoulder. Figure 3 shows the compressible pressure coefficient obtained using the present approach and a purely finite-difference technique.[7,12] Table 1 shows some more comparisons.

The most complicated problem solved using the developed formulation was the flow around a 9%-thick symmetric Joukowski airfoil. The region outside the airfoil was mapped conformally onto the computational domain which was the region outside a circular cylinder. The grid system consists of 48 equally spaced points in θ direction and of 40 points in r direction. The points in r direction are placed according to the exponential relation mentioned in Sec. III with $\Delta z = 0.164$, $S_0 = -2.88$ and $C = 0.943$. Figures 4 and 5 show the surface pressure distribution and vorticity of the airfoil, at zero angle of attack, for the following conditions: freestream Mach number 0.4, Prandtl number 1, Reynolds number based on the airfoil chord 1000. The calculations were started by using the potential flow solution as the initial flowfield.

Table 2 Comparison of present results and Ref. 7

Flow feature	Present results	Ref. 7
Onset of separation	$T = 0.506$	$T = 0.584$
Cycle of vortex shedding begins at	$Ts = 1.943$	$Ts = 1.699$
Cycle of vortex shedding ends at	$Te = 8.423$	$Te = 7.373$
First appearance of trailing-edge bubble	$T = 3.171$	$T = 2.88$
Strouhal number (chord/v_∞ T cycle)	0.1547	0.17626
$C_{L\,\max}$	1.32	1.34
$C_{L\,\min}$	0.254	0.251
$C_{D\,\max}$	0.346	0.364
$C_{D\,\min}$	0.165	0.141

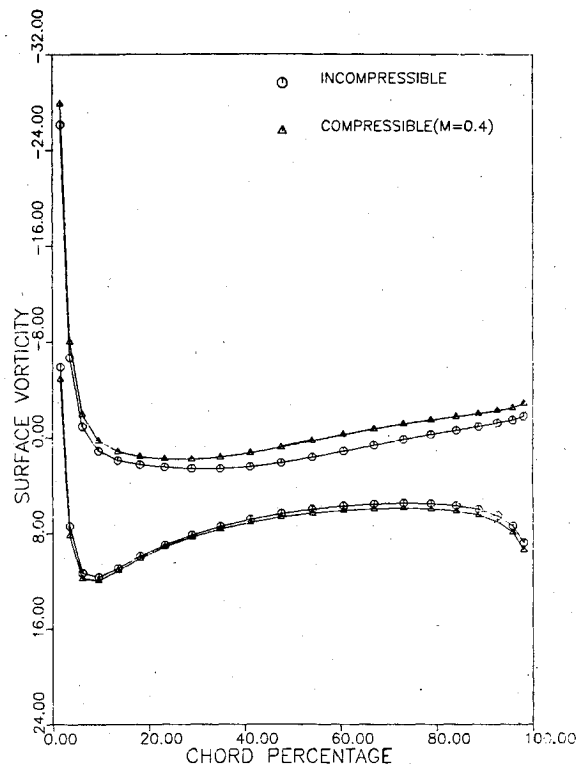

Fig. 7 Surface vorticity distribution for $T = 0.941$.

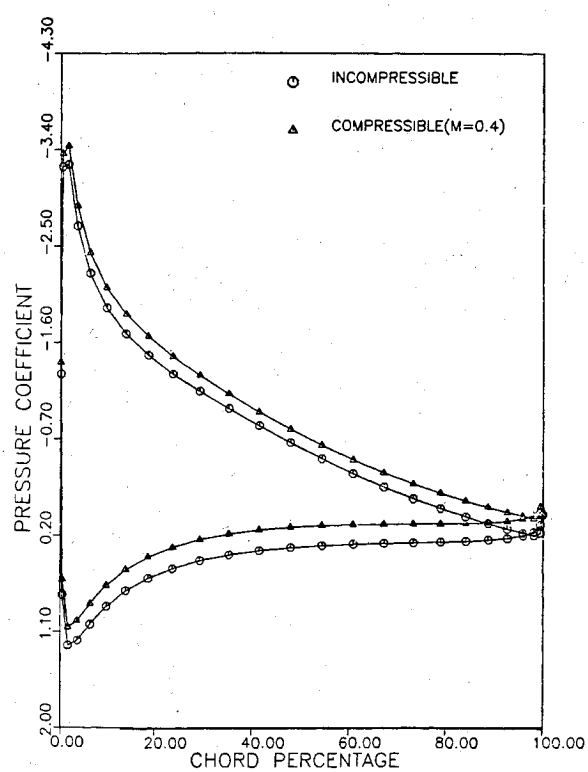

Fig. 6 Surface pressure distribution for $T = 0.941$.

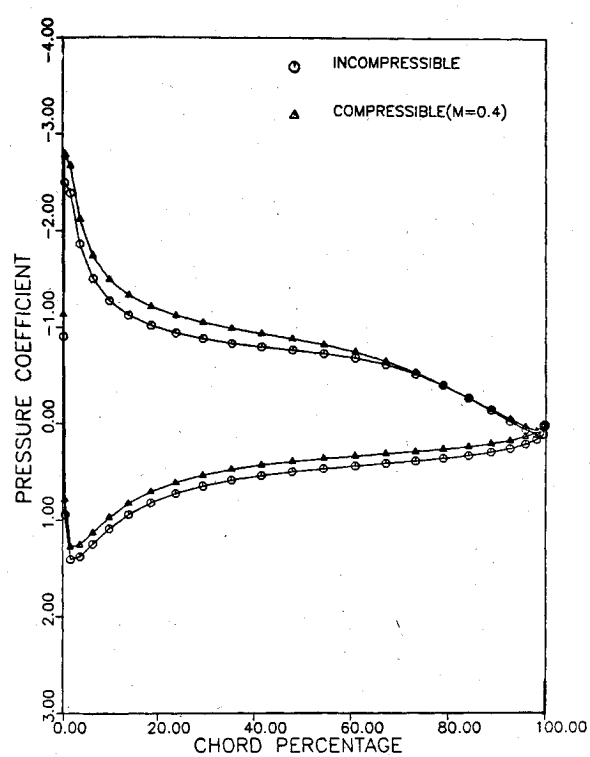

Fig. 8 Surface pressure distribution for $T = 2.557$.

Numerically steady state solution was obtained after a dimensionless time of 2.25, based on the freestream velocity and the airfoil chord. In Figs. 4 and 5 the surface pressure and vorticity distributions are compared with results of a purely finite-difference technique.[7,12] Considering the differences in the grids and the techniques used, the results are close. Similar comparisons for the angle-of-attack case were not always possible due to the different flowfields at the beginning of the calculations. Although the effect of the initial condition on the magnitude of the computed field variables decays rapidly, phase differences make further comparisons difficult. However some comparison between the present results and those of Ref. 7 is shown in Table 2. In the last test cases the solutions approach steady state asymptotically. However in the angle-of-attack case although the boundary conditions are independent of time, the solution obtained is unsteady (periodic behavior). The airfoil exhibited massive separation at 15-deg angle of attack. Figures 6-8 show the surface pressure distributions and Figs. 9-11 show the surface vorticity at three time levels after the beginning of the computations. Results for incompressible flow are also shown in these figures. The effect of compressibility, although small for the conditions stated previously, is to delay the sequence

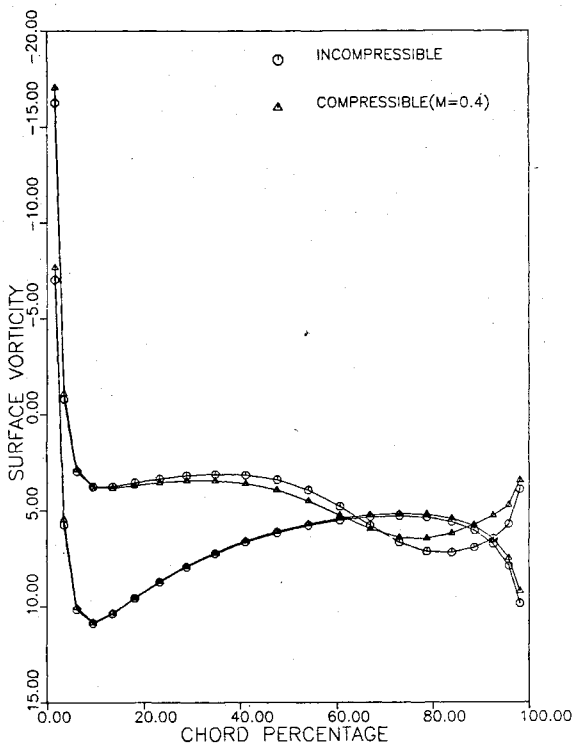

Fig. 9 Surface vorticity distribution for $T = 2.557$.

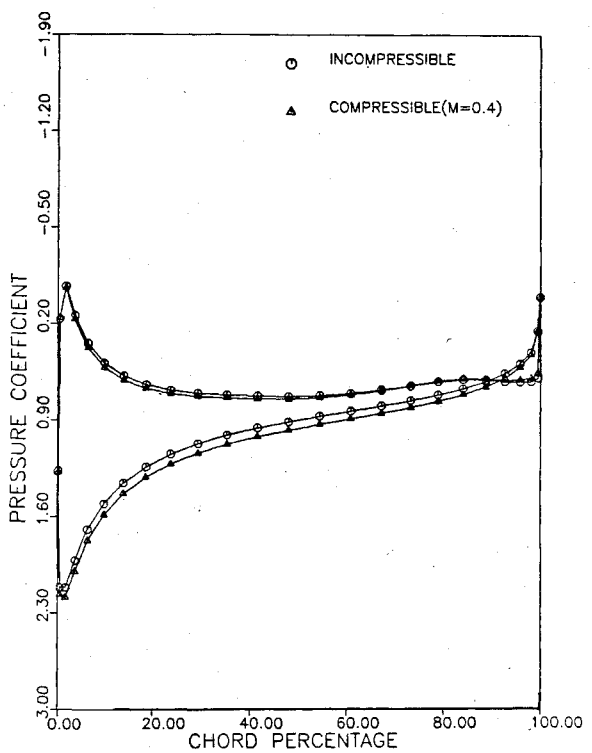

Fig. 10 Surface pressure distribution for $T = 5.013$.

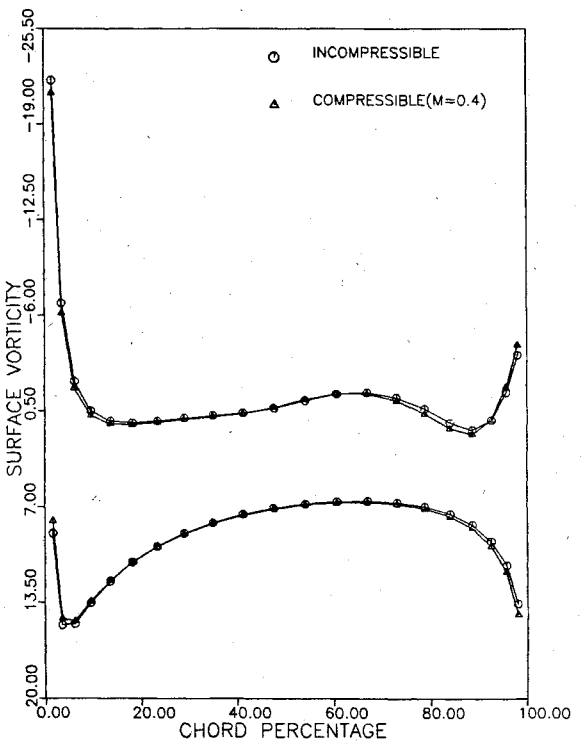

Fig. 11 Surface vorticity distribution for $T = 5.013$.

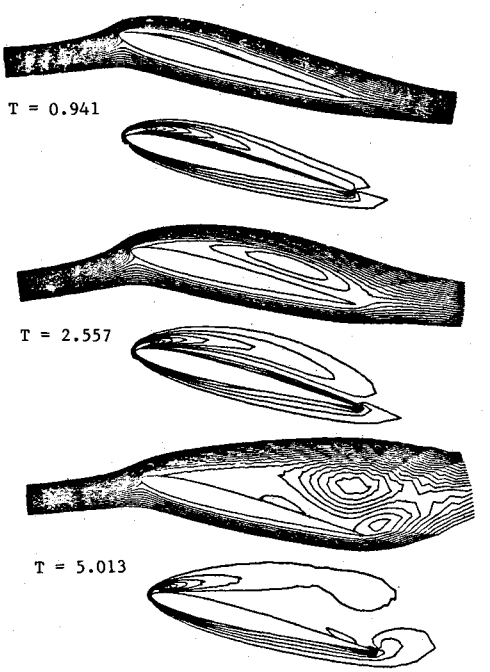

Fig. 12 Streamline-like lines and equal vorticity lines.

of events, like the growing of the bubble and the bursting of the bubble from the airfoil surface. Figure 12 shows the streamline-like lines at the same three time levels. These streamline-like lines were obtained using the stream function corresponding to the calculated vorticity, and a stream function corresponding to the potential flow due to the computed dilatation β, in an additive fashion.[11] For low Mach numbers, these lines are very close to the actual streamlines.

The grid was extended during the calculations due to the increasing viscous region of the flow. The average execution speed was 0.025 s per time step per grid point on a CDC 6600 computer. The whole cycle takes approximately 4.13 h.

V. Conclusions

The integral representation approach has been extended to the case of compressible flows, and has been used to solve the two-dimensional unsteady compressible Navier-Stokes equations for the following three subsonic test problems: the flow over a flat plate, around a circular cylinder, and around an airfoil. The solutions obtained compare favorably with existing finite-difference solutions. More important, the method restricts the domain of computations to the viscous region of the flowfield. The viscous region is the region where the vorticity and the difference in dilatation between the real flow and the potential flow around the body are numerically significant.

Appendix

$$\phi = -\omega\beta + \frac{\mu}{\rho^2 R_e}\,(4/3(\nabla\beta\times\nabla\rho)\cdot k - \nabla\rho\cdot\nabla\omega) + \frac{\gamma-1}{\gamma}\,\nabla\ell n\rho\times\nabla h + \frac{c_1}{R_e} \tag{A1}$$

$$c_1 = \frac{1}{\rho}(u_y+v_x)(\mu_{xx}-\mu_{yy}) + \frac{2}{\rho}(v_y-u_x)\mu_{xy} + \mu_x\left\{\frac{2}{\rho}\nabla^2 v + \frac{2}{\rho}u_{xy} - \frac{1}{\rho^2}\left(\rho_x u_y - v_x\rho_x - 2\rho_y u_x + \frac{2}{3}\rho_y\beta\right)\right\} + \mu_y\left\{-\frac{2}{\rho}\nabla^2 u + \frac{2}{\rho}v_{xy} - \frac{1}{\rho^2}\left(2\rho_x v_y - u_y\rho_y - v_x\rho_y - \frac{2}{3}\beta\rho_x\right)\right\} \tag{A2}$$

$$\psi = -(u_x^2+v_y^2+2u_y v_x) + \frac{\mu}{E^2 G_e}\left\{-\frac{4}{3}\nabla\rho\cdot\nabla\beta + (\nabla\rho x\nabla\omega)\cdot k\right\} - \frac{\gamma-1}{\gamma}(\nabla^2 h + h\nabla^2\ell n\rho + \nabla h\nabla\cdot\ell n\rho) + \frac{c_2}{R_e} \tag{A3}$$

$$c_2 = \frac{8}{3\rho}\nabla\beta\cdot\nabla\mu + \frac{2}{3}(\nabla\omega x\nabla\mu)\cdot k - \frac{2}{3\rho}\beta\nabla^2\mu + \frac{2}{\rho}(u_x\mu_{xx}+v_y\mu_{yy}) + (v_x+u_y)\mu_{xy} - \frac{1}{\rho^2}(v_x+\mu_y) + \rho_y\mu_x + \frac{2}{3}\frac{\beta}{\rho^2}(\nabla\rho\cdot\nabla\mu) - \frac{2}{\rho^2}(\rho_x u_x\mu_x + \rho_y v_y\mu_y) \tag{A4}$$

$$\theta = -(\gamma-1)\beta h + \frac{\gamma\mu}{\rho R_e}\left[\frac{\beta^2}{3} + (2u_x-\beta^2) + (2v_x-\omega)^2\right] + \frac{\gamma}{\rho R_e Pr}\nabla h\cdot\nabla k \tag{A5}$$

For low subsonic speeds the variation of viscosity has a negligible effect and the source terms can be approximated by

$$\phi = -\omega\beta + \frac{\mu}{R_e\rho^2}\left\{4/3(\nabla\beta\times\nabla\rho)\cdot k - \nabla\rho\cdot\nabla\omega\right\} + \frac{\gamma-1}{\gamma}(\nabla\ell n\rho\times\nabla h)\cdot k \tag{A6}$$

$$\psi = \beta^2 + (\nabla v\times\nabla u)\cdot k + \frac{\mu}{\rho^2 R_e}\left\{-4/3\nabla\rho\cdot\nabla\beta + (\nabla\rho\times\nabla\omega)\cdot k\right\} - \left(\frac{\gamma-1}{\gamma}\right)(\nabla^2 h + h\cdot\nabla^2\ell n\rho + \nabla h\cdot\nabla\ell n\rho) \tag{A7}$$

$$\theta = -(\gamma-1)\beta\cdot h + \frac{\mu\gamma}{\rho R_e}\left\{\left(\frac{4}{3}\right)\beta^2 + \omega^2 + 4(\nabla vx\nabla u)\cdot k\right\} \tag{A8}$$

In the preceding expression, k denotes the unit vector normal to the plane of the flow.

Acknowledgments

The work was supported by the Branch for Internal Computational Fluid Dynamics of the NASA Lewis Research Center through Grant NSG 3307.

References

[1]Metha, U. B. and Lavan, Z., "Starting Vortex, Separation Bubbles and Stall - A Numerical Study of Laminar Unsteady Flow Around an Airfoil," *Journal of Fluid Mechanics,* Vol. 67, Jan. 1975, pp. 227-256.

[2]Wu, J. C. and Sampath, S., "A Numerical Study of Viscous Flow Around an Airfoil," AIAA Paper 76-337, 1976.

[3]Metha, U. B., Paper 23, and Wu, J. C., Sampath, S., and Sankar, N. L., Paper 24, *Unsteady Aerodynamics, AGARD Conference Proceedings 227.*

[4]Sugavanam, A. and Wu, J. C., "Numerical Study of Separated Turbulent Flow over Airfoils," AIAA Paper 80-1441, 1980.

[5]Rizk, Y., "An Integral Representation Approach for Time-Dependent Viscous Flows," Ph.D. Thesis, Georgia Institute of Technology, Atlanta, Ga., 1980.

[6]Sankar, N. L. and Wu, J. C., "Viscous Flow Around Oscillating Airfoils - A Numerical Study," AIAA Paper 78-1225, 1978.

[7]Sankar, N. L. and Tassa, Y., "Reynolds Number and Compressibility Effects on Dynamic Stall of a NACA 0012 Airfoil," AIAA Paper 80-0010, Jan. 1980.

[8]Shamroth, S. J. and Gibeling, H. J., "The Prediction of the Turbulent Flow Field About an Isolated Airfoil," AIAA Paper 79-1543, 1979.

[9]Wu, J. C. and Thompson, J. F., "Numerical Solutions of Time-Dependent Incompressible Navier-Stokes Equations Using an Integro-Differential Formulation," *Journal of Computers and Fluids,* Vol. 1, No. 2, 1973, pp. 197-215.

[10]Wu, J. C., "Numerical Boundary Conditions for Viscous Flow Problems," *AIAA Journal,* Vol. 14, Aug. 1976, pp. 1042-1049.

[11]ElRefaee, M., "A Numerical Study of Laminar Unsteady Compressible Flow over Airfoils," Ph.D. Thesis, Georgia Institute of Technology, Atlanta, Ga., 1981.

[12]Sankar, N. L., private communication, Lockheed Georgia Co., Marietta, Ga., Jan. 1980.

[13]Wu, J. C., "Integral Representation of Field Variables for the Finite Element Solution of Viscous Flow Problems," *Proceedings of the 1974 Conference on Finite Element Method in Engineering,* Clarendon Press, 1974, pp. 827-840.

[14]Roach, P., *Computational Fluid Mechanics,* Hermosa Publishers, 1976, p. 73.

[15]Stewartson, K., "Correlated Incompressible and Compressible Boundary Layers," *Proceedings of the Royal Society,* Series A, Vol. 200, 1944, pp. 84-100.

[16]Grove, A. S., Shair, F. H., Peterson, E. E., and Acrivos, A., "An Experimental Investigation of the Steady Separated Flow Past a Circular Cylinder," *Journal of Fluid Mechanics,* Vol. 19, May 1964, pp. 60-80.